Strategies to Calculate Fukui Functions and Applications to Radicals with SOMO-HOMO Inversion

Pierpaolo Morgante and Jochen Autschbach*

Department of Chemistry University at Buffalo State University of New York Buffalo, NY 14260-3000, USA email: jochena@buffalo.edu

July 22, 2023

Abstract

This work introduces an efficient and numerically accurate procedure to calculate the Fukui function from fractional orbital occupation differences. The energy- and density-linearity conditions are investigated in the context of using optimally tuned (OT) range-separated hybrid (RSH) functionals for the calculation of the Fukui function. The methodology is then used to study the reactivity of organic radicals exhibiting energetic inversion between the singly occupied molecular orbital (SOMO) and the highest occupied molecular orbital (HOMO), that is, SOMO-HOMO inversion (SHI). The Fukui function correctly identifies the reactive sites of the molecules investigated, but additional computed quantities, such as radical reaction energies and vertical ionization potentials, are needed to distinguish SHI systems from conventional radicals.

1 Introduction

Density functional theory (DFT) in the Kohn–Sham (KS) formulation¹ is often considered the 'workhorse' among the first-principles quantum theoretical approaches aimed at understanding and predicting the reactivity of atoms and molecules from an energy perspective. Within the KS framework, conceptual density functional theory (C-DFT)² emerged as an alternative, by shifting the focus from the energy of a reaction to the analysis of the electron density and its derivatives. The most popular indicators used in C-DFT are the electronegativy,³ the chemical hardness and softness,⁴ and other response properties that describe how

the system reacts to changes. Among the latter, the *Fukui function* can be used to rationalize and predict the reactivity of a molecule, ^{5,6} and therefore it has received a lot of attention.

The Fukui function can be defined as the derivative of the electron density $\rho(\mathbf{r})$ with respect to the electron number N (treated as a continuous variable), with the derivative taken at a fixed external potential $v(\mathbf{r})$. The Fukui function inherits many of the properties of the electron density. For instance, it satisfies a cusp condition, it exhibits exponential asymptotic decay, and it is normalized. However, the derivative is discontinuous at integer N. Accordingly, the notation $f^+(\mathbf{r})$ and $f^-(\mathbf{r})$ indicates the derivative when approaching an integer N from above and below, respectively. Function $f^{+/-}(\mathbf{r})$ describes phenomena associated with an increase/decrease of the number of electrons. The two functions have also been interpreted as the tendency of a molecule—or a functional group within a molecule—to undergo, respectively, nucleophilic or electrophilic attack. An additional function $f^0(\mathbf{r})$ is defined as the average of f^+ and f^- , and it is typically used to understand the reactivity of a molecule towards radical (or 'neutral') attack. Hence, the family of Fukui functions is defined via

$$f(\mathbf{r})^{+/-/0} = \left(\frac{\partial \rho(\mathbf{r})}{\partial N}\right)_{\nu}^{+/-/0} \tag{1}$$

with '0' to be understood as the aforementioned $f^{+/-}$ average. In KS-DFT, assuming the exact KS functional, the energy and electron density of a system with fractional electron number $N + \delta$, with integer N and $0 \le \delta \le 1$, should behave as follows:

$$X(N+\delta) = (1-\delta)X(N) + \delta X(N+1) \quad ; \quad X = E \text{ or } \rho$$
 (2)

These *linearity conditions* for E and ρ assume a fixed external potential v; in other words, v(r) does not change with N or δ . The requirement of fixed v in Equations (1) and (2) implies that the same nuclear framework (charges, positions) must be used in all calculations for a given molecule. Practical calculations of the derivatives in Equation (1) usually use a finite difference approximation (FDA). Specifically, $\partial \rho/\partial N$ taken at integer N is in the FDA replaced by $[\rho(N+\delta)-\rho(N)]/\delta$. Instead of trying to approach the limit $\delta\to 0_\pm$ numerically, the FDA derivative can be taken with $\delta=\pm 1$ if the linearity condition for the density holds. This eliminates the requirement for explicit calculations with fractional electron numbers. Consequently, this constitutes the most common approach for calculating the Fukui function. Whether the FDA with $\delta=\pm 1$ is in fact a suitable strategy for practical approximate KS DFT calculations, where the linearity conditions do *not* usually hold, is an open question and among the topics of the present study.

Apart from the question whether the density linearity condition holds in approximate

KS calculations, a noted shortcoming of using the FDA is the difficulty of performing computations on anionic species.⁸ Under the approximation that the KS orbitals do not change upon variations in the electron number, i.e., a frozen-orbital approximation (FOA),²⁵ ('frozen core', in the words of Parr and Yang)⁵ and assuming the density linearity condition, the Fukui functions are given as

$$f_{\text{FOA}}^+ \simeq \rho_{\text{LUMO}} \; ; \; f_{\text{FOA}}^- \simeq \rho_{\text{HOMO}} \; ; \; f_{\text{FOA}}^0 \simeq [\rho_{\text{HOMO}} + \rho_{\text{LUMO}}]/2$$
 (3)

In the previous equation, LUMO stands for lowest unoccupied molecular orbital, HOMO is the highest occupied molecular orbital, and ρ is the corresponding density obtained from taking the absolute square (modulus) of the respective MO.^{5,26} Therefore, there is a direct, albeit approximate, relationship between the Fukui functions and frontier MO concepts, and when using Equation (3), only one calculation of the N-electron system is needed. Fukui functions are often 'condensed' to atoms.^{27–29} Typically, this is done using population analyses (Mulliken³⁰ or Hirshfeld charges³¹ are the most common), and therefore noticeably basis set-dependent. Alternatives that do not rely on population analyses have also been presented.^{32,33} Descriptors obtained with the frozen-orbital approximation are not generally accurate for molecules^{16,34,35} and will therefore not be considered further herein.

The linearity condition for the energy has been probed extensively. E(N) should be a series of straight line segments with derivative discontinuities at integer N. However, commonly used non-hybrid and global hybrid approximations such as PBE^{36} or $B3LYP^{37-39}$ give a smooth E(N) with positive curvature. Hartree–Fock (HF) calculations typically give negative curvature between integer-N points. Among many examples of this behavior shown in the literature, see References 40–43 and Figure 3 in the present article. The E(N) curvature is intimately tied to the KS delocalization error (DE), which itself has a close relationship with the self-interaction error (SIE) in approximate DFT. In comparison, the density (non)linearity has not received as much attention, despite the implications for the Fukui function.

When approximations to the exact functional are used, which is in all practical applications of KS-DFT, the Fukui function is (in the words of P. Ayers) 'accurate but not exact'. ^{8,45,46} The statement relates to two separate issues. One issue is that when the functional is approximate, so is the Fukui function calculated from Equation (1). The other issue is that the linearity conditions do not hold for approximate functionals. Non-linearity of $\rho(N)$ impacts the calculation of the Fukui function, such that errors arise, for instance, when using the FDA with $\delta=\pm 1$. ^{45,47,48}

Yang *et al.* previously computed analytical Fukui functions for the helium and beryllium atoms and the formaldehyde molecule with a local density approximation (LDA).⁴⁷ Good

agreement between the analytical results was obtained by FDA with $\delta = \pm 0.01$, whereas large deviations were obtained when adding or subtracting a full electron. The reason of this failure was attributed to the DE, and usage of such a small δ was recommended to avoid shortcomings. The issue of DE/SIE plagues essentially all modern functional approximations⁴¹ unless specific measures to remove it are adopted.^{49,50} It is known that a non-empirically optimally tuned^{43,50,51} range-separated hybrid (OT-RSH) functional produces close to piece-wise linearity of the energy, and there are indications that it also restores the density linearity condition. 'Two-dimensional' tuning further improves over standard OT-RSH by specifically optimizing piece-wise linearity of E(N). This means that OT-RSHs offer potentially significant improvements for calculations of the Fukui function. To calculate a Fukui function free from DE, Tozer and coworkers explored an OT-RSH for the carbon atom, its singly-charged anion, and its cations with charge up to +5, and tested their conclusions on the helium and beryllium atoms and on H₂CO.⁴⁰ Potential improvements from OT-RSHs were noted. A related analysis performed on the lithium, carbon, and fluorine atoms by Gould using 37 'conventional' functionals showed that most of them produce Fukui functions similar to those obtained with Quantum Monte Carlo calculations⁵³ without further modification, potentially because of favorable error cancellation among the electron densities.²³

This work aims at exploring numerical procedures to calculate the Fukui functions f^+ , f^- and f^0 accurately from fractional-N KS DFT calculations. The study is motivated in part by the scarcity of investigations of the density linearity condition in this context. Another motivation comes from recent reports of an unusually low reactivity, and therefore unusually high stability (in some cases postulated rather than observed), of organic radicals with energetic inversion of the HOMO and the singly occupied MO (SOMO).^{54,55} These reports raise the question whether SOMO-HOMO-inversion (SHI) radicals display Fukui functions that reflect reduced reactivity compared to non-SHI analogs. In Section 3, the computational approach is validated against the analytical data of Yang et al., and a suitable δ is identified. In Section 4, OT-RSH calculations are explored in the context of the density linearity condition, significantly expanding upon Reference 40. Additional applications are then reported in Section 5, focusing on radical systems. Specifically, it is investigated whether information from the Fukui function about the electronic structure of SHI systems is able to complement the orbital-based analyses used so far. It is found that the f^0 Fukui function correctly identifies the most reactive species, and that SHI does not necessarily translate into reduced reactivity. The comparison between the Fukui function-based prediction of reactivity and quantitative information in the form of computed bond dissociation energies further confirms the reliability of this indicator to obtain qualitative chemical information for SHI systems.

2 Theoretical and Computational Details

All calculations employed KS DFT. Geometry optimizations and frequency calculations were performed with the Gaussian 16 program, version A.03 (G16).⁵⁶ Molecular structures were characterized as minima based on harmonic vibrational frequency calculations. The NWChem program, version 7.0,⁵⁷ was used for the calculations involving fractional occupation numbers of orbitals, using the FON keyword implemented by one of us (JA) previously.^{43,58} The dplot run type of NWChem was used to generate cube format density data using one-, two-, and three-dimensional grids. Further manipulations of the cube data files, for example to generate the FDA Fukui functions, were carried out using the manipulatecube software developed in-house. *Mathematica* v. 13 notebooks⁵⁹ were used for visualizations. *Mathematica* notebooks for cube file visualizations and the manipulatecube source code are available free of charge at JA's GitHub page.⁶⁰

Data for analytical Fukui functions of helium, beryllium, and formaldehyde (H_2CO) were digitized from Reference 47 using the WebPlotDigitizer⁶¹ program and were used to test the numerical convergence of the FDA Fukui function calculations. The structure of H_2CO was optimized using the LDA functional SVWN5^{62,63} and the cc-pVQZ basis set⁶⁴ without f and g functions, here indicated as cc-pVQZ', to reproduce the calculations of Reference 47. All other molecules were optimized and characterized with the B3LYP-D3(BJ) functional^{37–39,65} and the def2-TZVP basis set.⁶⁶ This level of theory is known to produce high-quality molecular structures.^{67–72}

Convergence of the Fukui function of the H_2CO molecule with respect to the basis set was tested using the Weigend-Ahlrichs⁶⁶ and Dunning⁶⁴ families of basis sets with the SVWN5 functional. Basis sets ranging from double- ζ to augmented quadruple- ζ were tested, namely def2-XVP(D) (X=S, TZ, QZ) and (aug-)cc-pVnZ (n=D, T, Q). The Fukui functions were found to be converged at the triple- ζ level, and the def2-TZVP basis set was employed for the remainder of the calculations. Numerical tests using thresholds of 10^{-6} , 10^{-8} , and 10^{-10} au for the SCF convergence revealed no substantial impact on the calculation of the Fukui functions. The intermediate value of 10^{-8} au was therefore used. To minimize numerical errors arising from the integration grid, 73,74 the xfine/ultrafine grid specifications were chosen for all NWChem/G16 calculations. Selected benchmark data are reported in Section S1 of the Supporting Information (SI). For a subset of the studied systems, condensed Fukui functions were computed using the FDA approach with $\delta=0.10$ and the Mulliken density partitioning. 27,30 This partitioning, while being common, is not without shortcomings, $^{29,75-78}$ and for this reason we use the condensed values only as qualitative descriptors. Additional details are given in Section S2 of the SI. Numerical differences in the electron densities and

Fukui functions shown in Figures 4–7 are quantified using a root-mean-square integrated deviation σ_Z ($Z=\rho$ or f), calculated from the corresponding volume data as described in Section S3 of the SI.

System-specific OT-RSH parametrizations were determined as detailed in References 43 and 50, based on the LC-PBE functional 36,79 and are indicated herein as γ^* -LC-PBE. Regarding the need for a full long-range correction (LC) in the OT-RSH framework, see the discussion in Section 3.2 of Reference 58. For comparison with data from Reference 47, the cc-pVQZ' basis was used in the tuning of formaldehyde. The def2-TZVP basis was employed otherwise. The tuning procedure resulted in the determination of an optimal error-function range-separation parameter γ for each molecule. In a nutshell, for a parent system with N electrons, the range-separation parameter was determined so that the exact KS condition

$$\varepsilon_{\text{HOMO}}(x) + \text{IP}(x) = 0 \tag{4}$$

was satisfied as best as possible, with IP being the vertical ionization potential and x = N or N + 1. The γ parameters obtained in this way were used in the calculation of the f^- and f^+ Fukui functions of formaldehyde. The parameter γ employed for f^0 calculations was obtained⁸⁰ from adding the square of the left-hand side of Equation (4) for x = N and x = N + 1, followed by minimization with respect to γ . The full list of γ parameters is reported in Table S15 of the SI.

The energetic disposition for reactivity predicted by γ^* -LC-PBE was compared to the results of many additional functionals. These functionals belong to various rungs of what Perdew has referred to as *Jacob's ladder* of functional approximations, ⁸¹ with one generalized gradient approximation (GGA) [PBE-D3(BJ)^{36,65}], five meta-GGAs [B97M-V,^{82,83} M06-L,⁸⁴ M11-L,⁸⁵ MN15-L,⁸⁶ TPSS-D3(BJ)^{65,87}], two global hybrid GGAs [B3LYP-D3(BJ)^{37–39,65} and PBE0-D3(BJ)^{65,88,89}], three global hybrid meta-GGAs [M06-2X,⁹⁰ MN15,⁹¹ and TPSSh-D3(BJ)^{92,93}], four range-separated hybrid GGAs (ω B97X-D,⁹⁴ CAM-B3LYP⁹⁵ and the two versions of LC-PBE), and two RSH meta-GGAs (M11⁹⁶ and ω B97M-V^{83,97}). We note that the present study is not primarily a comparative benchmark of approximate functionals. The list of tested functional approximations covers many application scenarios, and the functionals have been subject to a variety of recent benchmark studies.^{93,98–100}

3 Validation of the Finite Difference Protocol

Published⁴⁷ analytical Fukui functions are used here to gauge the performance of the present FDA approach. In the case of the helium and beryllium atoms, the radial distribution of f^- ,

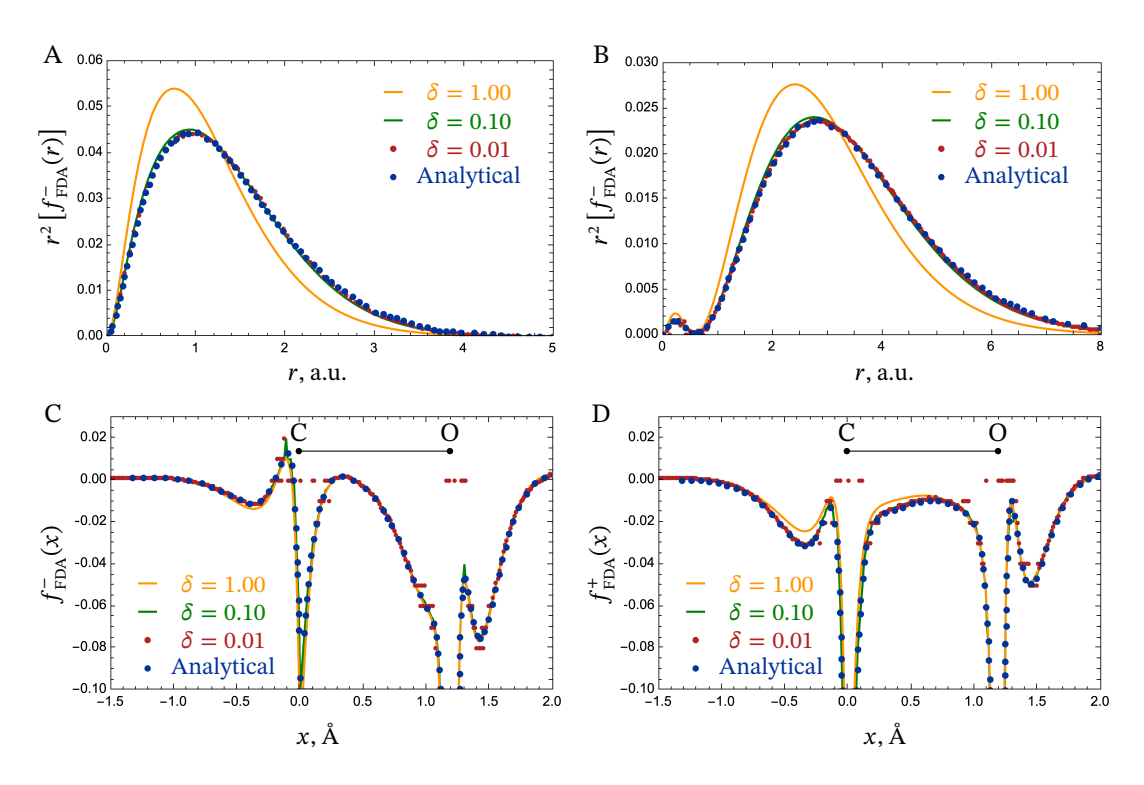


Figure 1: Top: Atomic Fukui functions. $r^2[f^-(r)]$ for the hydrogen and beryllium atoms (panels A and B). Bottom: Fukui functions for H_2CO . $f^-(x)$ and $f^+(x)$ (panels C and D) with x along the C–O axis. Present FDA results with different δ as indicated, vs. the analytical results digitized from Yang $et\ al.^{47}$ (blue dots).

that is, $r^2[f^-(r)]$ as a function of the electron-nucleus distance r is considered. In the case of formaldehyde, the functions f^+ and f^- were calculated along the axis containing the C-O bond (x), in the chosen coordinate system), indicated as $f^+_{\text{EDA}}(x)$ in Figure 1.

The FDA results obtained with $\delta=1.00$ are noticeably different from the analytical functions presented in Figure 1. Despite the fact that the addition and subtraction of a full electron is discouraged, ⁴⁷ this is still the most commonly used approach for calculating Fukui functions, especially in conjunction with the frozen orbital approximation, because it is very easy to set up these calculations. Fractional electron number calculations are not as widely supported by electronic structure programs, but Figure 1 shows that $\delta=\pm 1$ may lead to significant errors, whereas the analytic results and FDA with $\delta=0.10$ or 0.01 are virtually indistinguishable. In the present calculations with NWChem, using $\delta=0.01$ as recommended in Reference 47, or slightly larger values, appears to create numerical noise in some regions, especially for H_2CO close to the atomic nuclei. We confirmed that the commonly used technique of numerical grid-pruning is not responsible for the noise. Potentially, this happens because of other kinds of numerical cut-offs used to speed up the calculations. The Fukui functions obtained with $\delta=0.10$ are practically indistinguishable from the analytical

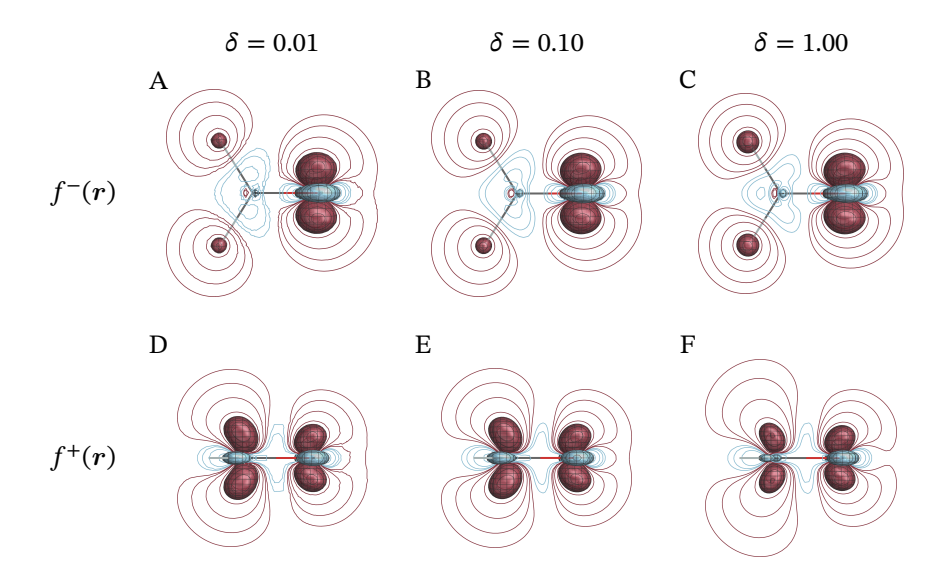


Figure 2: Isosurfaces (± 0.03 au) and contour maps ($\pm 0.003 \cdot 2^n$ au with n = 0, 1, 2... up to 7) for the Fukui functions of formaldehyde calculated with SVWN5/cc-pVQZ'. Top row: f^- viewed in the molecular plane (xy, z = 0) with different δ . Bottom row: f^+ viewed in the xz plane (y = 0).

functions, and therefore this value offers an excellent balance between numerical accuracy, stability, and efficiency in the FDA calculations.

Similar conclusions can be drawn based on comparisons in two (2D, in the form of contour line plots) and three dimensions (3D, in the form of iso-surfaces). For the 2D plots, we obtain FDA results with NWChem that are equivalent to those reported by Yang *et al.*^{14,47} Figure 2 shows the variations among the Fukui functions calculated with different values of δ . With $\delta = 1.00$, the Fukui functions are essentially free from numerical noise, but they also noticeably differ from those obtained with smaller δ . This reinforces the finding that such a large $\delta = 1.00$ is not generally suitable for quantitative evaluations. However, most of the differences between the Fukui functions obtained with large vs. small δ appear in the atomic cores.

To conclude this part of the investigation, the data show that $|\delta|=0.10$ will suffice for most practical applications of the fractional-electron FDA approach, producing essentially the same chemical information as FDA with $|\delta| \leq 0.01$ or analytical approaches, and without incurring unwanted numerical noise. Calculations with $\delta=\pm 1.00$, or the even cruder frozen-orbital approach invoking the HOMO and LUMO of a molecule, should probably be avoided. Yang et al. wrote in Reference 47 that the agreement between the FDA with reasonably small δ and the analytic results 'illustrates the validity of the analytic expressions'. One may also turn around the argument: The good agreement between analytic and FDA approaches validates the use of the latter in practical applications. The FDA has the advantage

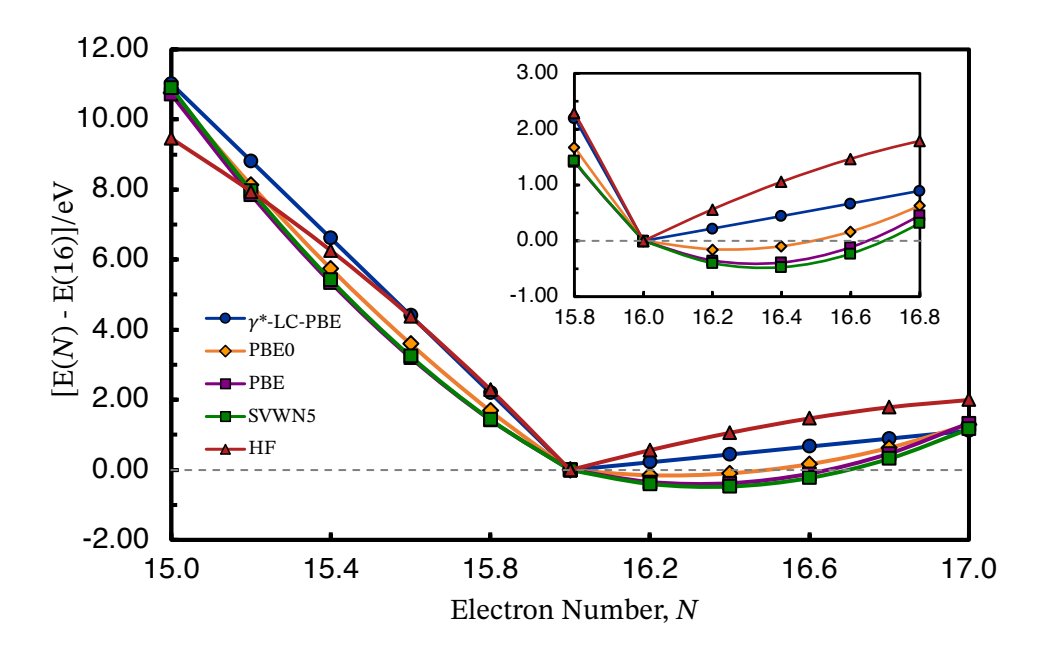


Figure 3: Total energy of formaldehyde, relative to the neutral molecule, as a function of the electron number N. Different functionals are indicated in the plot legend. The inset amplifies part of the plot. cc-pVQZ' basis set.

that it works the same when using non-hybrid or hybrid or RSH functionals, whereas the analytic implementation becomes more involved for functional approximations that have more 'ingredients'.

4 Density Linearity and OT-RSH Calculations

Empirically, it has been found that OT-RSHs cause the energy to follow the expected piecewise linear behavior quite closely, and the linearity itself can be a target of 'two-dimensional' tuning,⁵² as already mentioned. It remains to be seen whether the density linearity condition is also recovered by an OT-RSH. Figure 3 demonstrates that for the formaldehyde example, simple IP-based tuning produces the desired piece-wise linearity of E(N) (γ^* -LC-PBE data). The conventional functionals PBE, PBE0, and SVWN5 have a positive curvature, more so for the non-hybrid functionals, whereas HF gives negative curvature. This is an expected result, based on the previously cited literature on the topic.

To test the density linearity condition, the points with $\delta=\pm 0.5$ were selected, because there the deviations in the relative energies due to the curvature are most pronounced. This is even more evident in Figure S4 in the SI, which shows that the largest deviation from linearity is observed for SVWN5, closely followed by PBE. The deviation for PBE0 and HF is less pronounced, and it becomes vanishingly small for γ^* -LC-PBE. For the two fractional

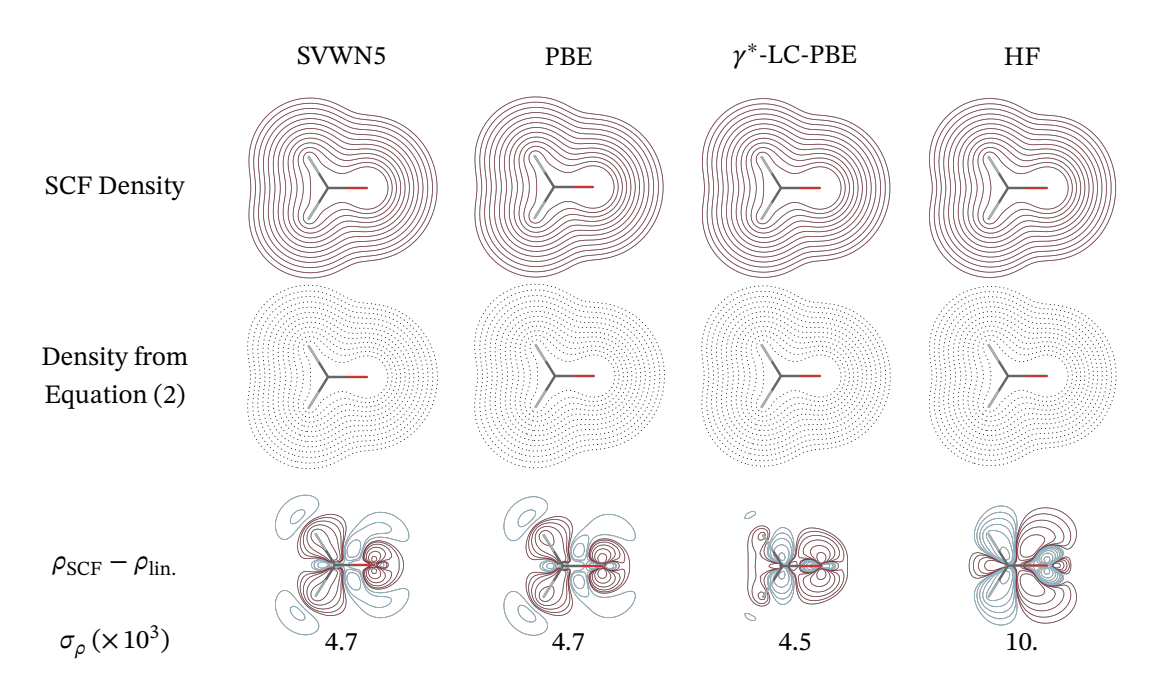


Figure 4: SCF densities (top row), densities obtained from the linearity condition [Equation (2), middle row], and the difference $\rho_{\text{SCF}} - \rho_{\text{lin.}}$ (bottom row) calculated for the $\text{H}_2\text{CO}^{+0.5}$ fractionally charged ion with different functionals. In the difference plots, blue/red contours represent a difference ≥ 0 . Contour lines: $\pm 0.003 \cdot 2^n$ au with $n = 0, 1, 2 \dots$ up to 11 for the densities, up to 3 for the differences. The σ_ρ values quantify the density differences (see Section S3 in the SI for details).

ions $H_2CO^{+0.5}$ and $H_2CO^{-0.5}$, the linearized (lin.) electron densities expected from Equation (2) are compared with the corresponding self-consistent (SC) densities in Figures 4 and 5 for the different functionals. Visual differences are hardly noticeable by comparing the contour line plots of the densities. We focus the discussion on the plots of $\rho_{\rm SCF}-\rho_{\rm lin.}$ aided by the σ_{ρ} indicators that quantify the differences between them. Even with contours going down to ±0.003, there is hardly any difference in the SCF versus linearized densities. It appears that adding (a fraction of) an electron causes less of a deviation from linearity than subtracting it, as shown by the plots for $\delta = \pm 0.5$ and by Figure S4 in the SI. HF performs the least well in regard to the density linearity, resulting in higher calculated σ_o values. There is no dramatic improvement from using an OT-RSH, although the latter does perform the best for $\delta = -0.5$. These findings came as a surprise, because the approximate functionals (other than OT-RSH) violate the energy linearity condition quite noticeably. It is visible from the plots for $\delta = +0.5$ that the differences in the sign of the E(N) curvature between HF and the density functionals goes along with a change in the sign of $\rho_{SCF} - \rho_{lin}$. In addition, the appearance of an increasing number of contour lines in the density difference plots is reflected in a larger magnitude of σ_{ρ} . It remains to be seen whether this correlation between the density and energy error is a

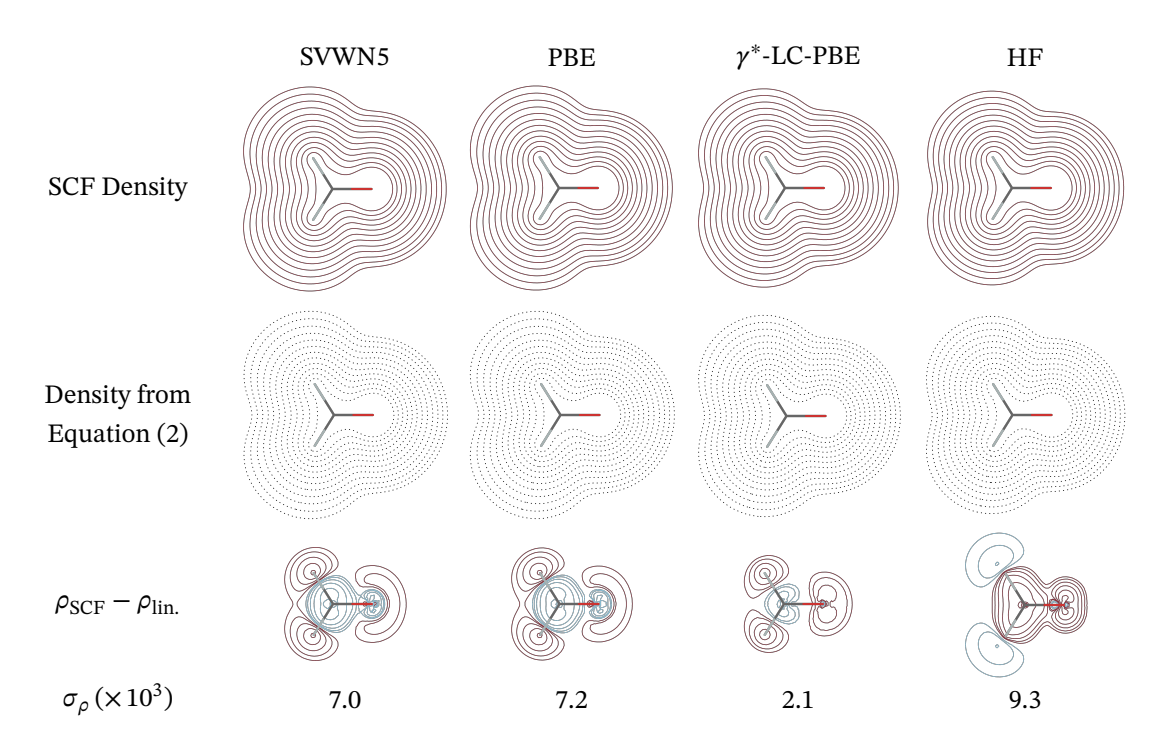


Figure 5: SCF densities (top row), densities obtained from the linearity condition [Equation (2), middle row], and density difference $\rho_{\text{SCF}} - \rho_{\text{linear}}$ (bottom row) calculated for the $\text{H}_2\text{CO}^{-0.5}$ fractionally charged ion with different functionals. In the difference plots, blue/red contours represent a difference ≥ 0 . Contour lines: $\pm 0.003 \cdot 2^n$ au with n = 0, 1, 2 ... up to 11 for the densities, up to 3 for the differences. The σ_{ρ} values quantify the density differences.

general feature or specific to the system studied here.

Presumably, the densities that are averaged together according to Equation (2) are reasonable references at integer N. This assumption is based on the energetic performance of approximate functionals, other than HF, which is generally not bad for the IP and the electron affinity (EA) of many compounds when calculated from total energy differences^{93,98} rather than orbital energies. This can be seen, for example, by the close agreement of the endpoints of the curves other than HF in Figure 3. With approximate functionals, Equation (2) is of course not fully satisfied for the densities, but as Gould pointed out,²³ it is possible that error cancellation in the density favorably affects the Fukui functions. In other words, small errors in the density may translate into significant errors in the energy, resulting—among other issues—in non-zero curvature of E(N), but for qualitative applications such as visual assessments of Fukui functions these errors may not be particularly significant.

The benefits of functional tuning become more evident in Figures 6 and 7, showing Fukui functions calculated with different values of δ in comparison to reference data calculated with $\delta=0.10$. As detailed in Section 3, the FDA with $\delta=0.10$ gives results that are deemed very close to the analytic Fukui functions, for the purpose of the present study. The OT-RSH is seen

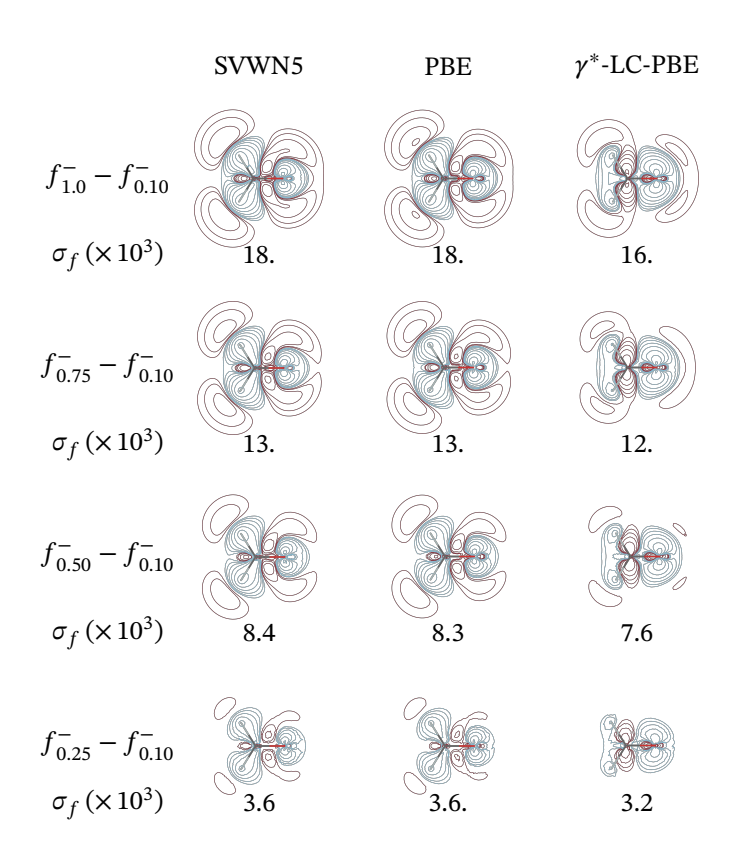


Figure 6: Differences in the FDA f^- functions in the molecular plane of formaldehyde, using $\delta=0.1$ as reference. cc-pVQZ' basis set. Red/blue contour lines indicate negative/positive function values. Contour lines values are $\pm 0.003 \cdot 2^n$ au with n=0,1,2... up to 3. The σ_f values quantify the Fukui function differences (see Section S3 in the SI for details).

to yield a consistent f^+ , whereas the non-hybrid functionals produce a noticeable dependence on the value chosen for δ , especially for $\delta \geq 0.50$, where the errors are particularly significant (σ_f larger than 10^{-2}). In the case of f^- , the differences in the calculated densities shown in Figure 4 are reflected in the Fukui function, suggesting that error cancellation—if present—is not as effective as for f^+ . As seen for the density differences, the magnitude of σ_f goes along with an increasing number of contour lines appearing in the $f^{+/-}$ difference plots, suggesting that visual examination of f^+ and f^- is sufficient to rationalize the qualitative aspects of the Fukui functions.

In addition to H_2CO , γ^* -LC-PBE also gives noticeable differences for values $\delta \geq 0.50$ of the f^- of two atoms, helium and beryllium (additional comments can be found in Section S6 of the SI). Good agreement between the functions obtained with $\delta = 0.10$ and $\delta = 1.00$ is found for beryllium (Figure S8). For helium, however, OT functionals do not improve upon conventional approximations much, mirroring the observed behavior for f^+ and f^- of formaldehyde. This shows that the energy linearity does not necessarily translate into

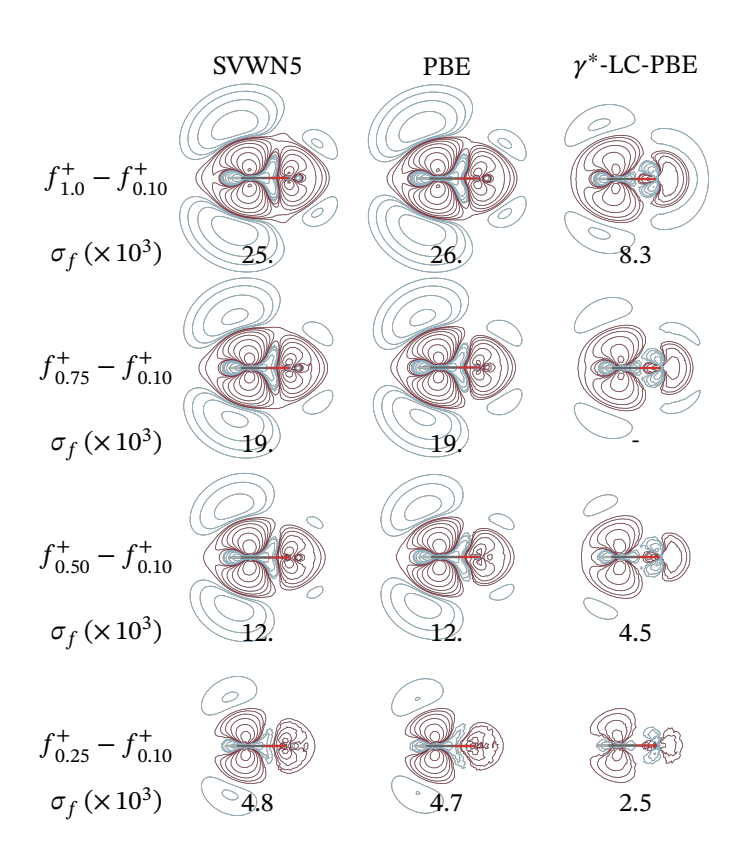


Figure 7: Differences in the f^+ functions calculated on the xz plane using $\delta=0.1$ as reference. The functionals used were SVWN5, PBE, γ^* -LC-PBE with the cc-pVQZ' basis set. Red/blue contour lines indicate negative/positive function values. In all cases, contour lines values are $\pm 0.003 \cdot 2^n$ au with n=0,1,2... up to 4. The σ_f values quantify the Fukui function differences.

density linearity. Reference 40 stated that the "energy-tuned parameter is applicable for the analogous density [linearity] condition". While OT does appear to lead to improvements with respect to the density linearity condition, however, our data show that it is still advisable to use small values of δ in FDA Fukui function calculations, even when using OT-RSHs.

5 Understanding the Reactivity of SHI Radicals

SHI radicals are characterized in spin-unrestricted calculations by a SOMO that is lower in energy than the α - β -pair of spin orbitals constituting the doubly occupied HOMO level. See References 54, 55, 101, 102 for details and examples. The unoccupied opposite-spin counterpart of the SOMO is labeled SUMO here and in related studies by us. The acronym stands for 'single unoccupied MO', to indicate that it has no corresponding opposite-spin counterpart in the unoccupied orbital space. It is also worth noting that the SOMO counterpart of the SUMO may have to be generated via a linear combination of several occupied same-spin MOs. ¹⁰² In

other words, a clear match between SOMO and SUMO may not be obtained straight from a self-consistent spin-unrestricted DFT calculation. This is not a restriction affecting the SHI classification, because linear combinations of same-spin occupied MOs can always be taken in spin-unrestricted KS DFT calculations, without loss of generality. In previous cases where linear combinations were necessary to bring about the SOMO-SUMO match, we found that the β -spin 'hole' in the spin density, for a calculation of a radical with $M_S=+1/2$, was well-reflected by the density of the SUMO. ¹⁰²

SHI does not occur in conventional radicals such as CH₃*, where the highest occupied spin orbital is the SOMO, but SHI may be much more common than previously thought. ¹⁰² It has been postulated that SHI goes along with increased radical stability and desirable photophysical behavior. However, it is so far unclear whether there is a correlation between SHI and the desired radical stability or properties. ⁵⁵ What is clear is that if the SHI gap (the SOMO-HOMO energy difference) is sufficiently large, then ionization of an SHI radical will result in an open-shell bi-radical rather than a closed-shell system. 'Sufficiently large' is a deliberately vague term. It is meant to indicate that SHI should be predicted consistently with a wide range of approximate functionals, such that it reflects in some way a real feature in the electronic structure, and that in a molecular orbital description of the system ionization occurs—as it should—from the HOMO.

Given the lack of understanding of SHI radicals, and the increasing interest in such systems, we thought it timely and important to assess whether the postulated stability of SHI radicals is reflected in the Fukui reactivity functions. The species selected for the analysis are the family of linear peroxyl radical anions ${}^{-}OOC-(CH_2)_n-O_2^{\bullet}$, with n=1 to 4, previously investigated in Reference 103, and the radical cation of 1-methylcytosine, 104 a derivative of one of the four constituents of DNA. Their reactivity is compared to closely related compounds that either exhibit partial or no SHI. The energetic aspect is tested using the (homolytic) $X-CH_3$ bond dissociation energies (BDEs, with X being an atom in the molecules), following a similar approach as was adopted in Reference 103, and calculated vertical IPs (reported and briefly discussed in Section S7 of the SI).

5.1 The Peroxyl Radical Family: Reactivity Towards CH₃

The reactivity of peroxyl radicals was extensively studied by Gryn'ova et al., 103 who established that the $^{-}OOC-(CH_2)_n-O_2^{\bullet}$ compounds exhibit SHI, and are less reactive than their protonated analogs, $HOOC-(CH_2)_n-O_2^{\bullet}$. We extend the investigation to include the two shortest-chain members of the series, namely $^{-}OOC-CH_2-O_2^{\bullet}$ and $^{-}OOC-CH_2-CH_2-O_2^{\bullet}$, and their protonated analogs $HOOC-CH_2-O_2^{\bullet}$ and $HOOC-CH_2-CH_2-O_2^{\bullet}$. For all radicals,

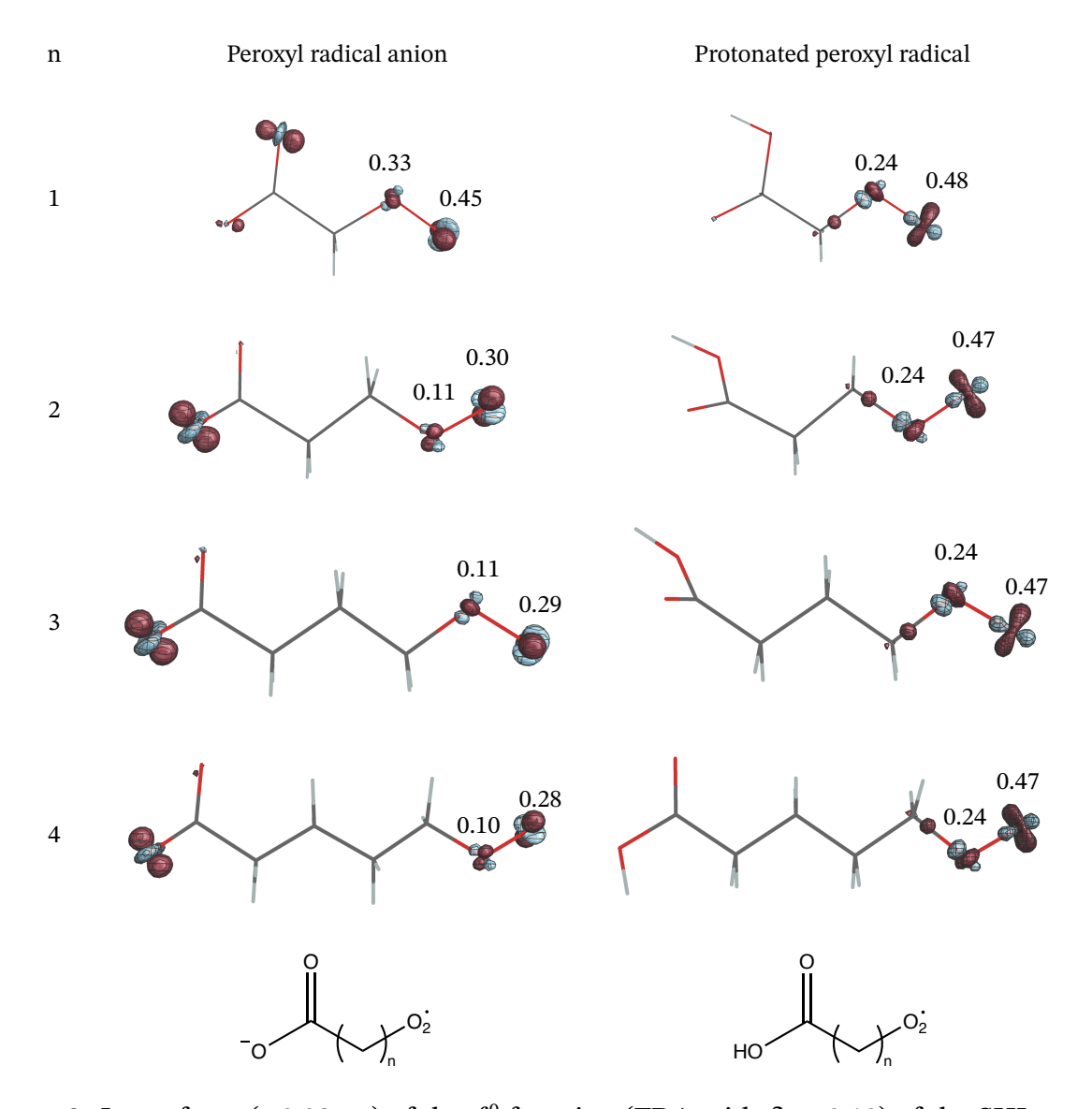


Figure 8: Isosurfaces (± 0.03 au) of the f^0 function (FDA with $\delta = 0.10$) of the SHI peroxyl radical anions (left) and their protonated analogs (right). γ^* -LC-PBE/def2-TZVP calculations with different values of γ^* depending on n (the numerical values are reported in Section S4 of the SI). The condensed Fukui functions are reported for selected atoms only.

the orbitals and the corresponding energies are reported in Figures S9-S20 in the SI.

The HOMO of the peroxyl radical anions is mostly localized on the carboxylate group, COO $^-$. The SOMO (and the corresponding SUMO) are localized on the superoxide group (O $_2^{\bullet}$) instead. These systems are designed as donor-radical pairs, with the carboxylate group being the donor and the superoxide being the radical, and the MOs reflect this property. The α - and β -HOMOs of the peroxyl radical anions are degenerate for practical purposes, with differences in the order of 0.01 eV (calculated with B3LYP, PBE0, and γ^* -LC-PBE, see SI). The SOMO-HOMO gap for the unprotonated radicals is rather large, 3 to 4 eV.

The SOMO of the protonated radicals is localized on the superoxo group, and it matches the SUMO. The HOMO is instead delocalized over the carboxylate and superoxo groups. Spatial separation from the SOMO is obtained only from the linear combination of HOMO and HOMO-2 (or HOMO-1 for the β spin-orbitals). The β -spin SUMO corresponds closely to the calculated α -spin density, as shown in the SI, Figure S21. The α -HOMO and SOMO are energetically quasi-degenerate, and they are lower than the β -HOMO by 0.4/0.5 eV. According to Reference 55, this orbital configuration, with the α and β spin HOMO noticeably differing in energy, classifies as *partial* SHI. Ionization of all the peroxyl radicals $^{-}$ OOC $^{-}$ (CH₂)_n $^{-}$ O₂ $^{\bullet}$ yields a triplet diradical (Tables S18 and S19 in the SI).

The f^0 Fukui functions calculated with $\delta = 0.10$ are shown in Figure 8. The functions calculated with $\delta = 1.00$ (Figure S22 in the SI) exhibit large values of σ_f for n = 1 and n = 13. Visual examination shows that this difference is only qualitative, as it is due to the way the Fukui function is localized on the carboxylate moiety. For $\delta = 0.10$, f^0 is localized on one oxygen atom, while for $\delta = 1.00$, the Fukui function is localized on the other oxygen. The two atoms are chemically identical, and the interpretation of the numerical indicator without prior visual examination of the Fukui functions is misleading, as the indicator does not account for chemical equivalence. For n = 2 and n = 4, the plots appear more similar instead. This observation further underlines the complementary relationship between visual examination of the Fukui function and numerical quantifications using σ_f or some other suitable indicators, and it highlights once more the need for a small δ in FDA calculations. The f^0 function of the radical anions is delocalized on both the carboxylate and superoxo groups, and it reflects the spatial separation of the orbitals. Upon protonation, f^0 becomes more localized, mirroring the changes observed in the MOs. The Fukui function identifies the superoxo as the main target for a radical attack, as it should, and its magnitude is larger for the protonated species, as shown numerically by the condensed values reported for the peroxo group in Figure 8. Visual comparison of the Fukui functions calculated with $\delta = 0.10$ and 1.00 for the protonated peroxyl radicals is shown in Figure S23 in the SI. The value of the σ_f indicator of those species is similar, and no substantial differences due to the choice of δ emerge. The length of the alkyl chain has no apparent influence on f^0 , as expected given the lack of π -conjugation between the donor and radical moieties. The condensed values describe this trend qualitatively, but they appear to be slightly overestimated for the shortest peroxyl radical anion (top left of Figure 8).

The qualitative features of f^0 are reflected quantitatively in the calculated bond dissociation energies collected in Table 1. Within both series of molecules, the BDEs vary only little as a function of the alkyl chain length, irrespective of the functional used. Furthermore, the BDEs calculated for the protonated species are larger than those of the radical anions, by

Table 1: Homolytic $O-CH_3$ bond dissociation energies (BDEs) of $^-OOC-(CH_2)_n-O_2-CH_3$ [HOOC- $(CH_2)_n-O_2-CH_3$ in parentheses] for n=1, 2, 3, 4 calculated with different functionals

| • | | | | |
|-------------------------|-------------------|-------------------|-------------------|-------------------|
| Functional ^a | BDE^b , $n = 1$ | BDE^b , $n = 2$ | BDE^b , $n = 3$ | BDE^b , $n = 4$ |
| PBE-D3(BJ) | 62.2 (69.7) | 61.6 (68.8) | 61.7 (68.3) | 60.7 (68.1) |
| B97M-V | 63.0 (70.1) | 63.5 (68.6) | 64.2 (68.9) | 63.7 (68.7) |
| M06-L | 60.9 (68.0) | 61.0 (66.6) | 61.6 (66.7) | 61.0 (66.7) |
| M11-L | 65.2 (70.9) | 65.6 (69.0) | 66.4 (69.8) | 66.3 (69.9) |
| MN15-L | 65.6 (72.2) | 66.2 (71.0) | 67.1 (71.0) | 66.9 (71.0) |
| TPSS-D3(BJ) | 58.9 (66.4) | 58.8 (65.5) | 59.3 (65.0) | 58.5 (64.8) |
| B3LYP-D3(BJ) | 59.4 (67.3) | 60.5 (66.1) | 61.5 (66.0) | 62.3 (65.7) |
| PBE0-D3(BJ) | 60.7 (68.5) | 62.0 (67.1) | 62.8 (67.1) | 63.7 (67.0) |
| M06-2X | 65.8 (74.1) | 67.4 (72.5) | 68.2 (72.7) | 69.1 (72.5) |
| MN15 | 66.2 (74.0) | 67.7 (72.6) | 68.5 (72.7) | 69.4 (72.6) |
| TPSSh-D3(BJ) | 58.5 (66.1) | 59.3 (65.1) | 60.4 (64.8) | 60.7 (64.6) |
| ω B97X-D | 60.9 (68.9) | 62.5 (67.7) | 63.3 (67.6) | 64.2 (67.5) |
| LC - PBE^c | 65.0 (73.9) | 66.9 (71.9) | 67.9 (72.5) | 68.8 (72.3) |
| γ^* -LC-PBE d | 67.1 (75.8) | 69.0 (74.2) | 70.0 (74.6) | 70.9 (74.4) |
| CAM-B3LYP | 59.5 (68.1) | 61.0 (66.4) | 61.9 (66.7) | 62.8 (66.3) |
| M11 | 63.4 (72.0) | 65.1 (70.1) | 65.8 (70.5) | 66.7 (70.1) |
| ωB97M-V | 64.0 (72.0) | 65.6 (70.7) | 66.4 (70.7) | 67.2 (70.6) |

^adef2-TZVP basis set; ^bValues in kcal/mol; $^{c}\gamma = 0.30 \text{ au}^{-1}$;

around 8 kcal/mol, confirming that protonation renders the radicals more reactive, although not dramatically so. The overall performance of the different functionals is very consistent, and the calculations reproduce the trends noted previously by Gryn'ova et al. 103 These authors also pointed out that the distonic nature of the peroxyl radicals renders the molecules more polarizable, and this effect was identified as the origin of the observed radical stability. 105 Our results demonstrate, additionally, that the higher reactivity of the protonated radicals is reflected in the magnitude of f^0 around the peroxo functional group. The increased polarizability of the radical anions goes along with a delocalization of the Fukui function on the peroxo and carboxylate groups. Therefore, the f^0 identifies the reactive site in the molecules, and the relative reactivity toward radical reactions, thus characterizing these systems qualitatively and semi-quantitatively.

5.2 1-Methylcytosine and Analogs: Reactivity Towards CH₃

The radical cation of 1-methylcytosine (molecule A in Figure 9) is one of many biologically relevant radicals that exhibit SHI. ¹⁰⁴ Five isoelectronic analogs were identified. Three

^dDifferent values of γ^* depending on n, see SI, Table S15.

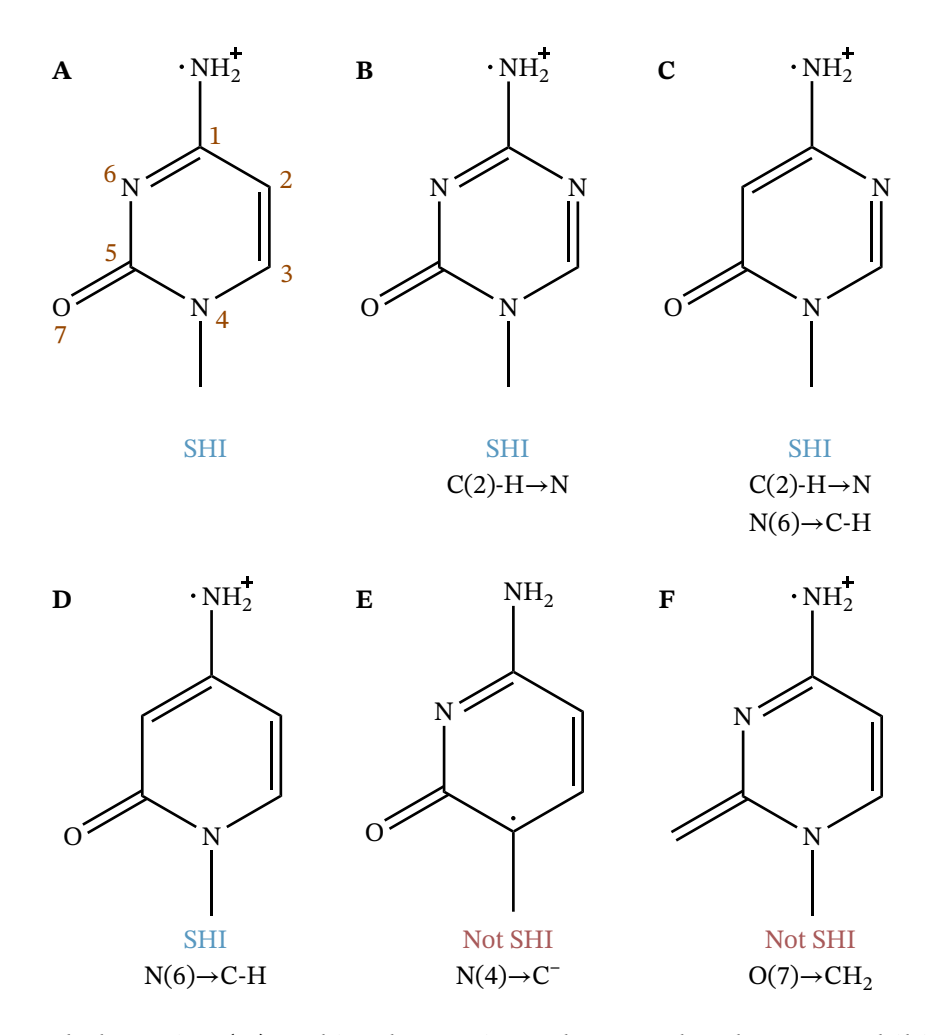


Figure 9: 1-methylcytosine (**A**) and isoelectronic analogs. Molecules **B**–**D** exhibit SHI, while molecules **E** and **F** do not. The atoms or groups replaced relative to **A** are indicated below each structure. The numbering of the atoms was chosen for convenience, and it does not follow standard naming rules.

(molecules \mathbf{B} – \mathbf{D}) display SHI, whereas molecules \mathbf{E} and \mathbf{F} are conventional radicals, as shown by their orbitals and orbital energies reported in Section S10 of the SI, and by the calculated IPs of Table S20 in the SI. Molecule \mathbf{F} , obtained by replacing the oxygen atom in position 7 of 1-methylcytosine with a methylene group (CH₂), was chosen for comparison with 1-methylcytosine because it offers the least change in the electronic structure (the other molecule without SHI, \mathbf{E} , is not charged).

The MOs of molecules $\bf A$ and $\bf F$ are very similar to each other. In 1-methylcytosine, the SOMO is lower in energy than the HOMO by ~0.5 eV. In molecule $\bf F$, the SOMO is the highest occupied MO, as typical for conventional radicals. In 1-methylcytosine, the frontier MOs are delocalized on the aromatic ring, with substantial contributions from O(7) and the NH₂ group. The spin density for this molecule closely resembles the square of the β SUMO, which

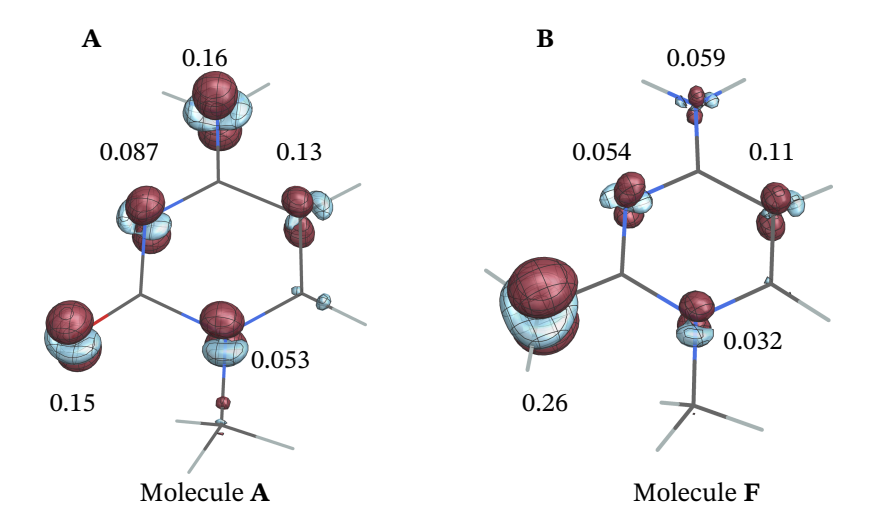


Figure 10: Isosurfaces (± 0.01 au) for the f^0 Fukui functions (FDA with $\delta = 0.10$) of 1-methylcytosine **A** (panel A) and analog **F** (panel B). γ^* -LC-PBE/def2-TZVP calculations with $\gamma = 0.2888$ au⁻¹ for panel A and 0.2647 au⁻¹ for panel B. The condensed Fukui functions are reported for selected atoms only.

is expected, as explained earlier. Replacing the oxygen with a CH_2 group $(\mathbf{A} \to \mathbf{F})$ localizes the MOs on the ring, decreasing the contributions from the substituents, as shown in Figure S42 in the SI. For molecule **F**, the β spin SUMO also reflects the calculated spin density (see Figure S42 in the SI). These similarities between molecules A and F are reflected in the reactivity pattern that emerges from panels A and B of Figure 10. The f^0 Fukui function indicates that different atoms or groups may be possible sites for radical attack, highlighting the ring nitrogens N(4) and N(6), and the ring carbon C(2) as common reactivity centers for the two molecules. Additional targets are the NH₂ group and oxygen O(7) in 1-methylcytosine and the CH_2 group in molecule **F**. Similar reactivity patterns emerge from the f^0 Fukui function of the other molecules, evidencing no substantial differences in their behavior towards radical attack (see Figure S43 in the SI). The same features are seen in the f^0 calculated with $\delta = 1.00$ (Figure S44 in the SI), and unlike the peroxyl radical anions, no noticeable differences emerge from the comparison of the results obtained with the two values of δ . Visual inspection of the Fukui function of molecule A reveals that the oxygen atom O(7) and the NH₂ group are the most reactive, followed by N(4), N(6), and C(2). For molecule **F**, the CH₂ group is the most reactive, followed by N(4), N(6), and C(2). It appears that the NH₂ group is not reactive. Notably, the condensed Fukui function values do not reflect the extensions of the lobes of f^0 plotted in Figure 10, but they correctly identify the most reactive atoms and groups $[CH_2 \text{ in molecule } \mathbf{F} \text{ and } O(7)/NH_2 \text{ in molecule } \mathbf{A}$. This apparent discrepancy is likely due to the limitations of the used Mulliken partitioning, as described for example in References 29, 78 and 106]. Overall, molecule A appears to be more reactive than F despite

$$NH_{2}^{\dagger}$$
 NH_{2}^{\dagger}
 NH_{2}
 NH_{2}

Figure 11: Reactions between a CH_3^{\bullet} radical and different atoms or groups of 1-methylcytosine (**A**, X=O) or analog **F** (X=CH₂) considered for the computation of the BDEs of Tables 2. See Table S21 for additional visuals.

the SHI character for the former.

The reactive sites identified by the f^0 Fukui function for molecules **A** and **F** were considered for reaction with a CH₃ radical, as shown in Figure 11. The corresponding BDEs are reported in Table 2. The different functionals predict that any atom in **A** is more reactive, thermodynamically, than its corresponding analog in molecule **F**. In fact, the BDEs of molecule **F** are lower than those in molecule **A** by ~ 30 kcal/mol. Thus, the BDEs indicating that SHI system **A** is more reactive than its non-SHI analog **F** clearly reflect the qualitative be-

Table 2: Homolytic bond dissociation energies (BDEs) for the methyl group of the CH_3^{\bullet} adducts of **A** (**F** in parentheses) calculated with different functionals. See also Figures 9 and 11.

| | BDE^a | BDE^a | BDE^a | BDE^a | BDE^a |
|-------------------------|------------------|------------------|------------------|------------------|---------------|
| Functional b | NH_2-CH_3 | $C(2)-CH_3$ | $N(4)-CH_3$ | $N(6)-CH_3$ | $O-CH_3$ |
| | | | | | (CH_2-CH_3) |
| PBE-D3(BJ) | 77.9 (54.5) | 64.6 (32.8) | 102.8 (66.5) | 72.7 (41.9) | 94.3 (87.8) |
| B97M-V | 75.8 (50.0) | 61.7 (28.0) | 100.9 (61.7) | 69.2 (35.7) | 94.7 (85.9) |
| M06-L | 74.8 (49.2) | 59.5 (25.2) | 100.2 (61.9) | 67.6 (35.0) | 92.3 (86.3) |
| M11-L | 76.8 (50.8) | 61.1 (27.7) | 100.9 (62.0) | 70.7 (37.6) | 94.3 (87.7) |
| MN15-L | 75.0 (48.0) | 61.3 (27.7) | 100.6 (60.2) | 69.9 (35.1) | 95.1 (85.0) |
| TPSS-D3(BJ) | 72.7 (48.5) | 60.6 (28.2) | 98.0 (60.6) | 68.7 (36.8) | 91.4 (82.0) |
| B3LYP-D3(BJ) | 75.6 (49.7) | 62.7 (29.4) | 101.3 (62.4) | 70.4 (37.1) | 94.3 (84.1) |
| PBE0-D3(BJ) | 79.2 (52.3) | 64.3 (30.4) | 105.6 (65.5) | 73.9 (39.3) | 98.1 (87.8) |
| M06-2X | 83.7 (55.3) | 70.6 (36.7) | 110.4 (69.3) | 79.2 (43.7) | 104.5 (90.4) |
| MN15 | 80.1 (53.3) | 67.2 (35.3) | 108.7 (69.2) | 75.7 (41.5) | 103.5 (88.9) |
| TPSSh-D3(BJ) | 73.7 (48.1) | 60.7 (27.6) | 99.5 (60.7) | 69.5 (36.2) | 93.2 (82.6) |
| ω B97X-D | 81.1 (52.9) | 65.9 (31.8) | 106.8 (66.1) | 75.3 (39.9) | 99.3 (89.2) |
| LC - PBE^c | 87.8 (57.3) | 70.3 (35.8) | 117.2 (73.7) | 81.5 (43.8) | 109.1 (95.0) |
| γ^* -LC-PBE d | 89.4 (61.9) | 74.3 (42.0) | 118.2 (78.3) | 84.6 (50.2) | 109.4 (98.7) |
| CAM-B3LYP | 76.5 (48.4) | 61.6 (27.2) | 103.3 (62.2) | 71.4 (36.2) | 97.5 (84.8) |
| M11 | 83.3 (54.1) | 69.4 (35.5) | 111.8 (70.0) | 78.8 (42.7) | 104.0 (90.7) |
| ωB97M-V | 83.5 (54.8) | 69.2 (35.6) | 108.4 (67.7) | 77.4 (42.1) | 102.2 (90.8) |

^aValues in kcal/mol; ^bdef2-TZVP basis set; $^{c}\gamma = 0.30 \text{ au}^{-1}$;

 $^{d}\gamma^{*} = 0.2888 \text{ au}^{-1} \text{ (molecule A) or } \gamma^{*} = 0.2647 \text{ au}^{-1} \text{ (molecule F)}.$

havior predicted by the Fukui function f^0 . Also, the magnitude of the Fukui function around the various centers matches the calculated BDEs qualitatively. The BDE calculations identify N(4) as the most reactive site, contradicting the f^0 prediction, but otherwise follow the reactivity order based on f^0 [O(7) ~ NH₂ > N(6) > C(2)]. For molecule **F**, the CH₂ group shows the largest BDE, and it is the most reactive site in the molecule, as predicted by f^0 . The Fukui function overestimates the reactivity of the NH₂ group, but it is qualitatively right regarding the other centers [N(4) > N(6) > C(2)].

6 Conclusions and Outlook

This work introduced a computationally and numerically practical procedure to calculate Fukui functions using the finite difference approximation. A finite-difference parameter value of $\delta=0.10$ was identified as a suitable best compromise between accuracy, numerical precision, and computational efficiency.

The benefits of optimally tuned functionals (OT-RSH) were examined using the formaldehyde molecule and two atoms. The tuning procedure restores the linearity conditions of the energy, but it provides less obvious improvements in the density compared to conventional approximations. However, there is no harm in studying Fukui functions obtained with OT-RSHs to predict chemical reactivity.

The FDA methodology was applied to study various compounds exhibiting SOMO-HOMO inversion (SHI) and to compare them with other radicals exhibiting partial or no SHI. In particular, we found that f^0 captures qualitative and semi-quantitative aspects of the reactivity of linear peroxyl radicals, but for 1-methylcytosine and its CH_2 -substituted analog the Fukui function only offers a rough qualitative description. Unless the latter systems are rare outliers, additional computed quantities such as bond dissociation energies and ionization potentials should accompany the f^0 Fukui function to obtain a quantitative description of the chemical reactivity of these systems. f^0 correctly identified 1-methylcytosine as more reactive than an isoelectronic non-SHI analog. Therefore, at least for this example, SHI is not in an obvious manner related to radical stability. It remains an open question whether 1-methylcytosine is an exception in this regard, or quite typical. Further research will be required to provide a definitive answer.

Acknowledgments

The Center for Computational Research (CCR) at the University at Buffalo is gratefully acknowledged for providing computational resources.¹⁰⁷ We thank the National Science Foundation for financial support of this research via grant CHE-2152633.

Supporting Information

Additional details on the convergence of the Fukui function with respect to the basis set size and different values of δ . Additional comments on the linearity condition in the He and Be atoms. Orbital plots and spin densities for the peroxyl radicals, 1-methylcytosine and its derivatives. Optimized geometries of all molecules.

References

[1] Kohn, W.; Sham, L. Self-Consistent Equations Including Exchange and Correlation Effects. *Phys. Rev. A* **1965**, *140*, 1133–1138.

- [2] Geerlings, P.; De Proft, F.; Langenaeker, W. Conceptual Density Functional Theory. *Chem. Rev.* **2003**, *103*, 1793–1874.
- [3] Parr, R. G.; Donnelly, R. A.; Levy, M.; Palke, W. E. Electronegativity: The Density Functional Viewpoint. *J. Chem. Phys.* **1978**, *68*, 3801–3807.
- [4] Parr, R. G.; Pearson, R. G. Absolute Hardness: Companion Parameter to Absolute Electronegativity. *J. Am. Chem. Soc.* **1983**, *105*, 7512–7516.
- [5] Parr, R. G.; Yang, W. Density Functional Approach to the Frontier-Electron Theory of Chemical Reactivity. *J. Am. Chem. Soc.* **1984**, *106*, 4049–4050.
- [6] Yang, W.; Parr, R. G. Hardness, Softness, and the Fukui Function in the Electronic Theory of Metals and Catalysis. *Proc. Natl. Acad. Sci. U.S.A.* **1985**, *82*, 6723–6726.
- [7] Chattaraj, P. K.; Cedillo, A.; Parr, R. G. Fukui Function from a Gradient Expansion Formula, and Estimate of Hardness and Covalent Radius for an Atom. *J. Chem. Phys.* **1995**, *103*, 10621–10626.
- [8] Ayers, P. W.; Levy, M. Perspective on "Density Functional Approach to the Frontier-Electron Theory of Chemical Reactivity". *Theor. Chem. Acc.* **2000**, *103*, 353–360.
- [9] Perdew, J. P.; Parr, R. G.; Levy, M.; Balduz, J. L. Jr. Density-Functional Theory for Fractional Particle Number: Derivative Discontinuities of the Energy. *Phys. Rev. Lett.* **1982**, *49*, 1691–1694.
- [10] Mori-Sánchez, P.; Cohen, A. J. The Derivative Discontinuity of the Exchange–Correlation Functional. *Phys. Chem. Chem. Phys.* **2014**, *16*, 14378–14387.
- [11] Fievez, T.; Sablon, N.; De Proft, F.; Ayers, P. W.; Geerlings, P. Calculation of Fukui Functions Without Differentiating to the Number of Electrons. 3. Local Fukui Function and Dual Descriptor. *J. Chem. Theory Comput.* **2008**, *4*, 1065–1072.
- [12] Grimmel, S. A.; Reiher, M. On the Predictive Power of Chemical Concepts. *Chimia* **2021**, 75, 311.
- [13] Yang, W.; Parr, R. G.; Pucci, R. Electron Density, Kohn–Sham Frontier Orbitals, and Fukui Functions. *J. Chem. Phys.* **1984**, *81*, 2862–2863.
- [14] Lee, C.; Yang, W.; Parr, R. G. Local Softness and Chemical Reactivity in the Molecules CO, SCN- and H2CO. *J. Mol. Struc.: THEOCHEM* **1988**, *163*, 305–313.

- [15] Langenaeker, W.; De Decker, M.; Geerlings, P.; Raeymaekers, P. Quantum-Chemical Study of the Fukui Function as a Reactivity Index: Probing the Acidity of Bridging Hydroxyls in Zeolite-Type Model Systems. *J. Mol. Struc.: THEOCHEM* **1990**, *207*, 115–130.
- [16] Langenaeker, W.; Demel, K.; Geerlings, P. Quantum-Chemical Study of the Fukui Function as a Reactivity Index. *J. Mol. Struc.: THEOCHEM* **1991**, *234*, 329–342.
- [17] Langenaeker, W.; Demel, K.; Geerlings, P. Quantum-Chemical Study of the Fukui Function as a Reactivity Index. *J. Mol. Struc.: THEOCHEM* **1992**, *259*, 317–330.
- [18] Ayers, P. W. Strategies for Computing Chemical Reactivity Indices. *Theor. Chem. Acc.* **2001**, *106*, 271–279.
- [19] Borgoo, A.; Tozer, D. J.; Geerlings, P.; De Proft, F. Confinement Effects on Excitation Energies and Regioselectivity as Probed by the Fukui Function and the Molecular Electrostatic Potential. *Phys. Chem. Chem. Phys.* **2009**, *11*, 2862.
- [20] Sablon, N.; Mastalerz, R.; Proft, F. D.; Geerlings, P.; Reiher, M. Relativistic Effects on the Fukui Function. *Theor. Chem. Acc.* **2010**, *127*, 195–202.
- [21] Fuentealba, P.; Florez, E.; Tiznado, W. Topological Analysis of the Fukui Function. *J. Chem. Theory Comput.* **2010**, *6*, 1470–1478.
- [22] Geerlings, P.; Ayers, P. W.; Toro-Labbé, A.; Chattaraj, P. K.; De Proft, F. The Woodward–Hoffmann Rules Reinterpreted by Conceptual Density Functional Theory. *Acc. Chem. Res.* **2012**, *45*, 683–695.
- [23] Gould, T. What Makes a Density Functional Approximation Good? Insights from the Left Fukui Function. *J. Chem. Theory Comput.* **2017**, *13*, 2373–2377.
- [24] Yañez, O.; Báez-Grez, R.; Inostroza, D.; Pino-Rios, R.; Rabanal-León, W. A.; Contreras-García, J.; Cardenas, C.; Tiznado, W. Kick–Fukui: A Fukui Function-Guided Method for Molecular Structure Prediction. *J. Chem. Inf. Model.* **2021**, *61*, 3955–3963.
- [25] Chermette, H. Chemical Reactivity Indexes in Density Functional Theory. *J. Comput. Chem.* **1999**, *20*, 129–154.
- [26] Hoffmann, G.; Tognetti, V.; Joubert, L. Can Molecular and Atomic Descriptors Predict the Electrophilicity of Michael Acceptors? *J. Mol. Model.* **2018**, *24*, 281.

- [27] Yang, W.; Mortier, W. J. The Use of Global and Local Molecular Parameters for the Analysis of the Gas-Phase Basicity of Amines. *J. Am. Chem. Soc.* **1986**, *108*, 5708–5711.
- [28] Mendez, F.; Gazquez, J. L. Chemical Reactivity of Enolate Ions: The Local Hard and Soft Acids and Bases Principle Viewpoint. *J. Am. Chem. Soc.* **1994**, *116*, 9298–9301.
- [29] Bultinck, P.; Fias, S.; Van Alsenoy, C.; Ayers, P. W.; Carbó-Dorca, R. Critical Thoughts on Computing Atom Condensed Fukui Functions. *J. Chem. Phys.* **2007**, *127*, 034102.
- [30] Mulliken, R. S. Electronic Population Analysis on LCAO-MO Molecular Wave Functions. I. *J. Chem. Phys.* **1955**, *23*, 1833–1840.
- [31] Hirshfeld, F. L. Bonded-Atom Fragments for Describing Molecular Charge Densities. *Theor. Chim. Acta* **1977**, *44*, 129–138.
- [32] Chamorro, E.; Pérez, P. Condensed-to-Atoms Electronic Fukui Functions within the Framework of Spin-Polarized Density-Functional Theory. *J. Chem. Phys.* **2005**, *123*, 114107.
- [33] Sablon, N.; De Proft, F.; Ayers, P. W.; Geerlings, P. Computing Fukui Functions without Differentiating with Respect to Electron Number. II. Calculation of Condensed Molecular Fukui Functions. *J. Chem. Phys.* **2007**, *126*, 224108.
- [34] Bartolotti, L. J.; Ayers, P. W. An Example Where Orbital Relaxation Is an Important Contribution to the Fukui Function. *J. Phys. Chem. A* **2005**, *109*, 1146–1151.
- [35] Anderson, J. S. M.; Melin, J.; Ayers, P. W. Conceptual Density-Functional Theory for General Chemical Reactions, Including Those That Are Neither Charge- nor Frontier-Orbital-Controlled. 2. Application to Molecules Where Frontier Molecular Orbital Theory Fails. *J. Chem. Theory Comput.* **2007**, *3*, 375–389.
- [36] Perdew, J. P.; Burke, K.; Ernzerhof, M. Generalized Gradient Approximation Made Simple. *Phys. Rev. Lett.* **1996**, *77*, 3865–3868.
- [37] Becke, A. D. Density-functional exchange-energy approximation with correct asymptotic behavior. *Phys. Rev. A* **1988**, *38*, 3098–3100.
- [38] Lee, C.; Yang, W.; Parr, R. G. Development of the Colle-Salvetti correlation-energy formula into a functional of the electron density. *Phys. Rev. B* **1988**, *37*, 785–789.
- [39] Becke, A. D. Density–functional thermochemistry. III. The role of exact exchange. *J. Chem. Phys.* **1993**, *98*, 5648–5652.

- [40] Gledhill, J. D.; De Proft, F.; Tozer, D. J. Range-Separation Parameter in Tuned Exchange-Correlation Functionals: Successive Ionizations and the Fukui Function. *J. Chem. Theory Comput.* **2016**, *12*, 4879–4884.
- [41] Lonsdale, D. R.; Goerigk, L. The One-Electron Self-Interaction Error in 74 Density Functional Approximations: A Case Study on Hydrogenic Mono- and Dinuclear Systems. *Phys. Chem. Chem. Phys.* **2020**, *22*, 15805–15830.
- [42] Johnson, E. R.; Otero-de-la Roza, A.; Dale, S. G. Extreme density-driven delocalization error for a model solvated-electron system. *J. Chem. Phys.* **2013**, *139*, 184116.
- [43] Autschbach, J.; Srebro, M. Delocalization error and 'functional tuning' in Kohn-Sham calculations of molecular properties. *Acc. Chem. Res.* **2014**, *47*, 2592–2602.
- [44] Cohen, A. J.; Mori-Sánchez, P.; Yang, W. Challenges for Density Functional Theory. *Chem. Rev.* **2012**, *112*, 289–320.
- [45] Michalak, A.; De Proft, F.; Geerlings, P.; Nalewajski, R. F. Fukui Functions from the Relaxed Kohn-Sham Orbitals. *J. Phys. Chem. A* **1999**, *103*, 762–771.
- [46] Ayers, P. W.; De Proft, F.; Borgoo, A.; Geerlings, P. Computing Fukui Functions without Differentiating with Respect to Electron Number. I. Fundamentals. *J. Chem. Phys.* **2007**, *126*, 224107.
- [47] Yang, W.; Cohen, A. J.; De Proft, F.; Geerlings, P. Analytical Evaluation of Fukui Functions and Real-Space Linear Response Function. *J. Chem. Phys.* **2012**, *136*, 144110.
- [48] Heidar-Zadeh, F.; Miranda-Quintana, R. A.; Verstraelen, T.; Bultinck, P.; Ayers, P. W. When Is the Fukui Function Not Normalized? The Danger of Inconsistent Energy Interpolation Models in Density Functional Theory. *J. Chem. Theory Comput.* **2016**, 12, 5777–5787.
- [49] Perdew, J. P.; Zunger, A. Self-interaction correction to density-functional approximations for many-electron systems. *Phys. Rev. B* **1981**, *23*, 5048–5079.
- [50] Baer, R.; Livshits, E.; Salzner, U. Tuned Range-Separated Hybrids in Density Functional Theory. *Ann. Rev. Phys. Chem.* **2010**, *61*, 85–109.
- [51] Refaely-Abramson, S.; Sharifzadeh, S.; Govind, N.; Autschbach, J.; Neaton, J. B.; Baer, R.; Kronik, L. Quasiparticle spectra from a non-empirical optimally-tuned range-separated hybrid density functional. *Phys. Rev. Lett.* **2012**, *109*, 226405 (5 pages).

- [52] Srebro, M.; Autschbach, J. Does a Molecule-Specific Density Functional Give an Accurate Electron Density? The Challenging Case of the CuCl Electric Field Gradient. *J. Phys. Chem. Lett.* **2012**, *3*, 576–581.
- [53] Gould, T.; Toulouse, J. Kohn-Sham Potentials in Exact Density-Functional Theory at Noninteger Electron Numbers. *Phys. Rev. A* **2014**, *90*, 050502.
- [54] Murata, R.; Wang, Z.; Abe, M. Singly Occupied Molecular Orbital-Highest Occupied Molecular Orbital (SOMO-HOMO) Conversion. *Aust. J. Chem.* **2021**, *74*, 827.
- [55] Kasemthaveechok, S.; Abella, L.; Crassous, J.; Autschbach, J.; Favereau, L. Organic radicals with inversion of SOMO and HOMO energies and potential applications in optoelectronics. *Chem. Sci.* **2022**, *13*, 9833–9847.
- [56] Frisch, M. J.; Trucks, G. W.; Schlegel, H. B.; Scuseria, G. E.; Robb, M. A.; Cheeseman, J. R.; Scalmani, G.; Barone, V.; Petersson, G. A.; Nakatsuji, H.; Li, X.; Caricato, M.; Marenich, A. V.; Bloino, J.; Janesko, B. G.; Gomperts, R.; Mennucci, B.; Hratchian, H. P.; Ortiz, J. V.; Izmaylov, A. F.; Sonnenberg, J. L.; Williams-Young, D.; Ding, F.; Lipparini, F.; Egidi, F.; Goings, J.; Peng, B.; Petrone, A.; Henderson, T.; Ranasinghe, D.; Zakrzewski, V. G.; Gao, J.; Rega, N.; Zheng, G.; Liang, W.; Hada, M.; Ehara, M.; Toyota, K.; Fukuda, R.; Hasegawa, J.; Ishida, M.; Nakajima, T.; Honda, Y.; Kitao, O.; Nakai, H.; Vreven, T.; Throssell, K.; Montgomery, J. A. Jr.; Peralta, J. E.; Ogliaro, F.; Bearpark, M. J.; Heyd, J. J.; Brothers, E. N.; Kudin, K. N.; Staroverov, V. N.; Keith, T. A.; Kobayashi, R.; Normand, J.; Raghavachari, K.; Rendell, A. P.; Burant, J. C.; Iyengar, S. S.; Tomasi, J.; Cossi, M.; Millam, J. M.; Klene, M.; Adamo, C.; Cammi, R.; Ochterski, J. W.; Martin, R. L.; Morokuma, K.; Farkas, O.; Foresman, J. B.; Fox, D. J. "Gaussian 16 Revision C.01", Gaussian, Inc., Wallingford CT, 2016. URL: www.gaussian.com.
- [57] Aprà, E.; Bylaska, E. J.; de Jong, W. A.; Govind, N.; Kowalski, K.; Straatsma, T. P.; Valiev, M.; van Dam, H. J. J.; Alexeev, Y.; Anchell, J.; Anisimov, V.; Aquino, F. W.; Atta-Fynn, R.; Autschbach, J.; Bauman, N. P.; Becca, J. C.; Bernholdt, D. E.; Bhaskaran-Nair, K.; Bogatko, S.; Borowski, P.; Boschen, J.; Brabec, J.; Bruner, A.; Cauët, E.; Chen, Y.; Chuev, G. N.; Cramer, C. J.; Daily, J.; Deegan, M. J. O.; Dunning, T. H.; Dupuis, M.; Dyall, K. G.; Fann, G. I.; Fischer, S. A.; Fonari, A.; Früchtl, H.; Gagliardi, L.; Garza, J.; Gawande, N.; Ghosh, S.; Glaesemann, K.; Götz, A. W.; Hammond, J.; Helms, V.; Hermes, E. D.; Hirao, K.; Hirata, S.; Jacquelin, M.; Jensen, L.; Johnson, B. G.; Jónsson, H.; Kendall, R. A.; Klemm, M.; Kobayashi, R.; Konkov, V.;

- Krishnamoorthy, S.; Krishnan, M.; Lin, Z.; Lins, R. D.; Littlefield, R. J.; Logsdail, A. J.; Lopata, K.; Ma, W.; Marenich, A. V.; Martin del Campo, J.; Mejia-Rodriguez, D.; Moore, J. E.; Mullin, J. M.; Nakajima, T.; Nascimento, D. R.; Nichols, J. A.; Nichols, P. J.; Nieplocha, J.; Otero-de-la Roza, A.; Palmer, B.; Panyala, A.; Pirojsirikul, T.; Peng, B.; Peverati, R.; Pittner, J.; Pollack, L.; Richard, R. M.; Sadayappan, P.; Schatz, G. C.; Shelton, W. A.; Silverstein, D. W.; Smith, D. M. A.; Soares, T. A.; Song, D.; Swart, M.; Taylor, H. L.; Thomas, G. S.; Tipparaju, V.; Truhlar, D. G.; Tsemekhman, K.; Van Voorhis, T.; Vázquez-Mayagoitia, Á.; Verma, P.; Villa, O.; Vishnu, A.; Vogiatzis, K. D.; Wang, D.; Weare, J. H.; Williamson, M. J.; Windus, T. L.; Woliński, K.; Wong, A. T.; Wu, Q.; Yang, C.; Yu, Q.; Zacharias, M.; Zhang, Z.; Zhao, Y.; Harrison, R. J. NWChem: Past, present, and future. *J. Chem. Phys.* 2020, 152, 184102 (27 pages).
- [58] Srebro, M.; Autschbach, J. Tuned Range-Separated Time-Dependent Density Functional Theory applied to Optical Rotation. *J. Chem. Theory Comput.* **2012**, *8*, 245–256.
- [59] *Mathematica* computer algebra software, Wolfram Research. URL http://www.wolfram.com, accessed 01/2023.
- [60] URL https://github.com/jautschbach (accessed 01/2023).
- [61] Rohatgi, A. "WebPlotDigitizer", 2016 http://arohatgi.info/WebPlotDigitizer, v3.10.
- [62] Slater, J. C. A Simplification of the Hartree-Fock-Method. *Phys. Rev.* **1951**, *3*, 385–390.
- [63] Vosko, S. H.; Wilk, L.; Nusair, M. Accurate spin-dependent electron liquid correlation energies for local spin density calculations: a critical analysis. *Can. J. Phys.* **1980**, *58*, 1200–1211.
- [64] Dunning, T. H. Gaussian basis sets for use in correlated molecular calculations. I. The atoms boron through neon and hydrogen. *J. Chem. Phys.* **1989**, *90*, 1007–1023.
- [65] Grimme, S.; Ehrlich, S.; Goerigk, L. Effect of the damping function in dispersion corrected density functional theory. *J. Comput. Chem.* **2011**, *32*, 1456–1465.
- [66] Weigend, F.; Ahlrichs, R. Balanced basis sets of split valence, triple zeta valence and quadruple zeta valence quality for H to Rn: Design and assessment of accuracy. *Phys. Chem. Chem. Phys.* **2005**, *7*, 3295–3305.

- [67] Witte, J.; Goldey, M.; Neaton, J. B.; Head-Gordon, M. Beyond Energies: Geometries of Nonbonded Molecular Complexes as Metrics for Assessing Electronic Structure Approaches. *J. Chem. Theory Comput.* **2015**, *11*, 1481–1492.
- [68] Kesharwani, M. K.; Brauer, B.; Martin, J. M. L. Frequency and Zero-Point Vibrational Energy Scale Factors for Double-Hybrid Density Functionals (and Other Selected Methods): Can Anharmonic Force Fields Be Avoided? *J. Phys. Chem. A* **2015**, *119*, 1701–1714.
- [69] Sirianni, D. A.; Alenaizan, A.; Cheney, D. L.; Sherrill, C. D. Assessment of Density Functional Methods for Geometry Optimization of Bimolecular van Der Waals Complexes. *J. Chem. Theory Comput.* **2018**, *14*, 3004–3013.
- [70] Hanson-Heine, M. W. D. Benchmarking DFT-D Dispersion Corrections for Anharmonic Vibrational Frequencies and Harmonic Scaling Factors. *J. Phys. Chem. A* 2019, 123, 9800–9808.
- [71] Morgante, P.; Peverati, R. CLB18: A New Structural Database with Unusual Carbon–Carbon Long Bonds. *Chem. Phys. Lett.* **2021**, 765, 138281.
- [72] Morgante, P.; Ludowieg, H. D.; Autschbach, J. Comparative Study of Vibrational Raman Optical Activity with Different Time-Dependent Density Functional Approximations: The VROA36 Database. *J. Phys. Chem. A* **2022**, *126*, 2909–2927.
- [73] Wheeler, S. E.; Houk, K. Integration grid errors for meta-GGA-predicted reaction energies: Origin of grid errors for the M06 suite of functionals. *J. Chem. Theory Comput.* **2010**, *6*, 395–404.
- [74] Morgante, P.; Peverati, R. The Devil in the Details: A Tutorial Review on Some Undervalued Aspects of Density Functional Theory Calculations. *Int. J. Quantum Chem.* **2020**, e26332.
- [75] Kinkar Roy, R.; Hirao, K.; Krishnamurty, S.; Pal, S. Mulliken Population Analysis Based Evaluation of Condensed Fukui Function Indices Using Fractional Molecular Charge. *J. Chem. Phys.* **2001**, *115*, 2901–2907.
- [76] Tiznado, W.; Chamorro, E.; Contreras, R.; Fuentealba, P. Comparison among Four Different Ways to Condense the Fukui Function. *J. Phys. Chem. A* **2005**, *109*, 3220–3224.

- [77] Fitzgerald, G. On the Use of Fractional Charges for Computing Fukui Functions. *Mol. Simul.* **2008**, *34*, 931–936.
- [78] Saha, S.; Roy, R. K.; Ayers, P. W. Are the Hirshfeld and Mulliken Population Analysis Schemes Consistent with Chemical Intuition? Consistency of HPA and MPA Schemes with Chemical Intuition. *Int. J. Quantum Chem.* **2009**, *109*, 1790–1806.
- [79] Iikura, H.; Tsuneda, T.; Yanai, T.; Hirao, K. A long-range correction scheme for generalized-gradient-approximation exchange functionals. *J. Chem. Phys.* **2001**, *115*, 3540–3544.
- [80] Kuritz, N.; Stein, T.; Baer, R.; Kronik, L. Charge-Transfer-Like $\pi \to \pi^*$ Excitations in Time-Dependent Density Functional Theory: A Conundrum and Its Solution. *J. Chem. Theory Comput.* **2011**, 7, 2408–2415.
- [81] Perdew, J. P.; Schmidt, K. Jacob's ladder of density functional approximations for the exchange-correlation energy. *AIP Conf. Proc.* **2001**, *577*, 1–20.
- [82] Mardirossian, N.; Head-Gordon, M. Mapping the Genome of Meta-Generalized Gradient Approximation Density Functionals: The Search for B97M-V. *J. Chem. Phys.* **2015**, *142*, 074111–32.
- [83] Vydrov, O. A.; Van Voorhis, T. Nonlocal van der Waals density functional: The simpler the better. *J. Chem. Phys.* **2010**, *133*, 244103(9).
- [84] Zhao, Y.; Truhlar, D. G. A New Local Density Functional for Main-Group Thermochemistry, Transition Metal Bonding, Thermochemical Kinetics, and Noncovalent Interactions. *J. Chem. Phys.* **2006**, *125*, 194101.
- [85] Peverati, R.; Truhlar, D. G. M11-L: A Local Density Functional That Provides Improved Accuracy for Electronic Structure Calculations in Chemistry and Physics. *J. Phys. Chem. Lett.* **2012**, *3*, 117–124.
- [86] Yu, H. S.; He, X.; Truhlar, D. G. MN15-L: A New Local Exchange-Correlation Functional for Kohn–Sham Density Functional Theory with Broad Accuracy for Atoms, Molecules, and Solids. *J. Chem. Theory Comput.* **2016**, *12*, 1280–1293.
- [87] Tao, J.; Perdew, J. P.; Staroverov,; Scuseria, G. E. Climbing the density functional ladder: Nonempirical Meta-Generalized Gradient Approximation designed for molecules and solids. *Phys. Rev. Lett.* **2003**, *91*, 146401.

- [88] Adamo, C.; Barone, V. Toward reliable density functional methods without adjustable parameters: The PBE0 model. *J. Chem. Phys.* **1999**, *110*, 6158–6170.
- [89] Ernzerhof, M.; Scuseria, G. E. Assessment of the Perdew–Burke–Ernzerhof exchange-correlation functional. *J. Chem. Phys.* **1999**, *110*, 5029–5036.
- [90] Zhao, Y.; Truhlar, D. G. The M06 suite of density functionals for main group thermochemistry, thermochemical kinetics, noncovalent interactions, excited states, and transition elements: two new functionals and systematic testing of four M06-class functionals and 12 other functionals. *Theor. Chem. Acc.* **2008**, *120*, 215–241.
- [91] Yu, H. S.; He, X.; Li, S. L.; Truhlar, D. G. MN15: A Kohn–Sham Global-Hybrid Exchange–Correlation Density Functional with Broad Accuracy for Multi-Reference and Single-Reference Systems and Noncovalent Interactions. *Chem. Sci.* **2016**, *7*, 5032–5051.
- [92] Staroverov, N. V.; Scuseria, G. E.; Tao, J.; Perdew, J. P. Comparative assessment of a new nonempirical density functional: Molecules and hydrogen-bonded complexes. *J. Chem. Phys.* **2003**, *119*, 12129–12137.
- [93] Goerigk, L.; Hansen, A.; Bauer, C.; Ehrlich, S.; Najibi, A.; Grimme, S. A Look at the Density Functional Theory Zoo with the Advanced GMTKN55 Database for General Main Group Thermochemistry, Kinetics and Noncovalent Interactions. *Phys. Chem. Phys.* **2017**, *19*, 32184–32215.
- [94] Chai, J.-D.; Head-Gordon, M. Long-Range Corrected Hybrid Density Functionals with Damped Atom–Atom Dispersion Corrections. *Phys. Chem. Chem. Phys.* **2008**, *10*, 6615.
- [95] Yanai, T.; Tew, D. P.; Handy, N. C. A new hybrid exchange-correlation functional using the Coulomb-attenuating method (CAM-B3LYP). *Chem. Phys. Lett.* **2004**, *393*, 51–57.
- [96] Peverati, R.; Truhlar, D. G. Improving the Accuracy of Hybrid Meta-GGA Density Functionals by Range Separation. *J. Phys. Chem. Lett.* **2011**, *2*, 2810–2817.
- [97] Mardirossian, N.; Head-Gordon, M. ωB97M-V: A Combinatorially Optimized, Range-Separated Hybrid, Meta-GGA Density Functional with VV10 Nonlocal Correlation. *J. Chem. Phys.* **2016**, *144*, 214110.
- [98] Mardirossian, N.; Head-Gordon, M. Thirty Years of Density Functional Theory in Computational Chemistry: An Overview and Extensive Assessment of 200 Density Functionals. *Mol. Phys.* **2017**, *115*, 2315–2372.

- [99] Mehta, N.; Casanova-Páez, M.; Goerigk, L. Semi-Empirical or Non-Empirical Double-Hybrid Density Functionals: Which Are More Robust? *Phys. Chem. Chem. Phys.* **2018**, 20, 23175–23194.
- [100] Najibi, A.; Goerigk, L. The Nonlocal Kernel in van Der Waals Density Functionals as an Additive Correction: An Extensive Analysis with Special Emphasis on the B97M-V and ω B97M-V Approaches. *J. Chem. Theory Comput.* **2018**, *14*, 5725–5738.
- [101] Gryn'ova, G.; Coote, M. L.; Corminboeuf, C. Theory and practice of uncommon molecular electronic configurations. *WIREs Comput. Mol. Sci.* **2015**, *5*, 440–459.
- [102] Abella, L.; Favereau, L.; Crassous, J.; Autschbach, J. Why is the energy of the singly occupied orbital in some radicals below the highest occupied orbital energy? *Chem. Mater.* **2021**, *33*, 3678–3691.
- [103] Gryn'ova, G.; Marshall, D. L.; Blanksby, S. J.; Coote, M. L. Switching radical stability by pH-induced orbital conversion. *Nat. Chem.* **2013**, *5*, 474–481.
- [104] Kumar, A.; Sevilla, M. D. SOMO-HOMO Level Inversion in Biologically Important Radicals. *J. Phys. Chem. B* **2018**, *122*, 98–105.
- [105] Gryn'ova, G.; Coote, M. L. Origin and Scope of Long-Range Stabilizing Interactions and Associated SOMO-HOMO Conversion in Distonic Radical Anions. *J. Am. Chem. Soc.* **2013**, *135*, 15392–15403.
- [106] Arulmozhiraja, S.; Kolandaivel, P. Condensed Fukui Function: Dependency on Atomic Charges. *Mol. Phys.* **1997**, *90*, 55–62.
- [107] Center for Computational Research, University at Buffalo, "UB CCR Support Portfolio,", 2020 http://hdl.handle.net/10477/79221.

Table of Contents Graphics

